THE ASTROPHYSICAL JOURNAL, 327:712–722, 1988 April 15


# GRAVITATIONAL LIGHT BENDING NEAR NEUTRON STARS. II. ACCRETING PULSAR SPECTRA AS A FUNCTION OF PHASE

P. MÉSZÁROS AND H. RIFFERT
Pennsylvania State University
*Received 1987 June 15; accepted 1987 October 6*

## ABSTRACT

We present X-ray pulse shapes and phase-dependent cyclotron spectra of simple accretion column and accretion cap models of rotating magnetized neutron stars, including general relativistic light-bending effects. We show that the latter effects can be strong, and discuss the beaming properties and phase-dependent spectral properties as a function of the stellar radius, using realistic magnetized input spectra. We show that a qualitatively correct fit to the observations of Her X-1 can be obtained only in two situations: either the accretion is of the cap (flat hot spot) type and the neutron star radius is larger than about 4 Schwarzschild radii, or else the accretion is of the column (protruding) type and the neutron star radius is of the order of 1.6 Schwarzschild radii. On the basis of various theoretical arguments and the current status of other evidence, the latter seems indicated at present.

*Subject headings:* gravitational lenses — pulsars — stars: accretion — stars: neutron — X-rays: binaries

## I. INTRODUCTION

In a previous paper (Riffert and Mészáros 1988, hereafter Paper I), we investigated the effects of light bending around neutron stars, without considering any detailed spectral effects. In accreting pulsars, the X-ray spectrum is rich in peculiarities associated with the presence of a strong magnetic field, which produces a distinctive angle and frequency behavior. In previous calculations of X-ray spectra of accreting pulsars (Mészáros and Nagel 1985*a*, *b*, hereafter MN1 and MN2), we discussed the flat-space radiative transfer calculations appropriate for an emitting surface where a strong magnetic field is perpendicular to the surface (cap geometry) or where the strong magnetic field is parallel to the surface (column geometry). These calculations gave the emergent spectrum as a function of angle and frequency in the frame appropriate to a particular radius, either the stellar radius or the radius of a particular height along the column. The spectrum as a function of angle for an observer at infinity will be modified, however, if the star is gravitationally compact enough, because of several effects (see Paper I). First, there is the general relativistic light bending, which affects differently rays emitted in different directions and from different heights, which causes a mixing of various rays. Since the spectra emitted at different angles are different, the final observed spectrum has a different angular behavior than in the flat-space case. Second, there is the occultation effect of the star and the column, as well as the other column, due to the fact that some of the curved photon paths intersect these surfaces (this effect is not present in the cap models, only in the columns). Third, there is the usual gravitational redshift, which in the case of the columns produces a final observed spectrum which is a combination of spectra emitted at different heights, differently redshifted. The frequency-integrated (bolometric) pulse shapes, and the response functions for a delta-function input in rest frequency, were discussed by us previously (Paper I). In the present paper we apply the curved space transport methods of Paper I, together with the magnetized radiative transfer methods of MN1 and MN2, to follow the changes in the accreting pulsar X-ray spectrum as a function of angle and frequency in the empty space around the neutron star, which is assumed to satisfy a Schwarzschild metric.

In § II we describe the basic models, assumptions, and calculation procedures for the cap and column models. The results for specific cases are given in § III, where the effect of varying different parameters such as the radius and the opening angle is investigated. The results are discussed and compared with observations in § IV. The *HEAO 1* and other data on the pulse shapes (White, Swank, and Holt 1983), and the *HEAO 1* and MPE/AIT balloon data on the cyclotron line centroids of Her X-1 as a function of phase (Voges *et al.* 1982) indicate that the models which best fit a high-luminosity Her X-1 type object are either a large radius ($R/R_S > 4$) polar cap (slab) model, or else a small-radius ($R/R_S < 2$), wide-angle accretion column. Various theoretical arguments lead to a preference for the latter option. In the low-luminosity accreting pulsars, it may be possible to discriminate between collisionless shock (column) and Coulomb decelerated (cap), models, e.g., Harding *et al.* (1984), if phase-dependent cyclotron line data become available for them in the future.

## II. CALCULATIONS

Neutron star radii depend on the equation of state (e.g., Baym and Pethick 1979), ranging from about 1.5 Schwarzschild radii (where the Schwarzschild radius is $R_S = 2GM/c^2 = 4.2M_{1.4}$ km for a 1.4 $M_\odot$ star) to about 4 Schwarzschild radii. As an input to our general relativistic transport calculations, we use a detailed model of the X-ray pulsar emission surface emergent flux, including magnetic effects on the spectrum and taking full account of the opacity-induced anisotropy. We have performed flat-space magnetized radiative transfer calculations for cap and column models with uniform density, temperature, and magnetic field strengths in the same range as models B and C of MN2, for two polarizations, 32 frequencies and eight angles. These arbitrary values are chosen to fit the observed spectrum of Her X-1, and are representative of a number of other X-ray pulsars (XRPs) (e.g., White, Swank, and Holt 1983). The density is 0.5 g cm$^{-3}$, the Thomson optical depth is 20, and the temperature and cyclotron ground energy are

chosen such that after gravitational redshift the mean comes out at $T_{\rm obs} = 8$ keV, $E_{c\,\rm obs} = 38$ keV. As described in paper MN2, the cap and column geometries, while leading to similar phase-averaged (or angle-averaged) spectra, give in the flat-space case a qualitatively very different phase-angle behavior of the spectrum. In particular, the cyclotron line width and line energy centroid increase or decrease with increasing flux as a function of angle, in such a manner as to allow one to decide between these two geometries, by comparing with the observed phase behavior (Voges *et al.* 1982). This was done in MN1 assuming that flat-space light propagation from the surface on outward was adequate, an assumption which is reasonably correct for stellar radii greater than about 4 $R_S$. Here, we want to investigate smaller neutron star radii, and therefore calculate the propagation of light in the space surrounding the emitting atmosphere using the methods appropriate for a Schwarzschild metric, described in Paper I.

It should be emphasized that our curved space propagation treatment is used only outside the emitting atmosphere. Inside it, the radiative transfer is complicated enough owing to the strong magnetic field effects to preclude for the moment the inclusion of space curvature effects. Our transport is therefore fully consistent only outside the atmosphere. What we assume is that our flat-space atmosphere spectrum (adequately redshifted) is an approximately adequate input for the subsequent general relativistic transport in the empty space outside the atmosphere. This approximation is probably very good for the polar cap models, where the atmosphere has a height much less than the stellar radius. It is less good, but probably still reasonably adequate, for the column models, where the photons may propagate inside the atmosphere over somewhat larger distances, although still usually smaller by an order of magnitude than a stellar radius, and on average traveling parallel to the surface, i.e., in regions of roughly constant redshift. When a fully consistent curved space magnetic transfer is possible, one may expect that the column output will contain a slightly larger proportion of photons which originally were emitted upward, since these will be less likely to be bent down toward the stellar surface inside the column. However, since the photons suffer many scatterings and changes of directions, this is not expected to affect the spectrum or output by much. In the case of the cap models, there should not be any significant changes.

The range of neutron star radii we investigate here ranges from values $R/R_S = 4$, where the behavior is close to the flat-space case, down to $R/R_S = 1.6$, close to the "photon radius" $R/R_S = 1.5$ at which photons emitted tangentially to the stellar surface orbit an infinite number of times (Misner, Thorne, and Wheeler 1973). In the case of the columns, the choice of the column upper radius $R_c$ determines, together with the stellar radius $R$, the total observed luminosity emitted into $4\pi$, since this is given by the surface specific emissivity multiplied by the total emitting area. The total luminosity at infinity is this, minus the fraction of the emitted radiation which is gravitationally recaptured by the star. Aside from the total normalization factor, the flux as a function of angle at infinity is most sensibly dependent on whether most of the emitting area is above or below the generalized gravitational focusing radius $R_\pi$. This radius (see Paper I) is defined as a function of the polar cap or column opening angle, and is given by the radius from which light emitted into a surface-grazing orbit reaches infinity at an angle which is 180° away from the (opposite, or hidden) magnetic axis direction. For the column models, the upper column radii have been chosen to give approximate agreement with the observed luminosity of typical XRPs, e.g., Her X-1 (Trümper *et al.* 1978), about (1–2) $\times 10^{37}$ erg s$^{-1}$. This choice leads to having most of the column below the focusing radius for the larger stellar radii, and most of the column above the focusing radius at the lower stellar radii (below about $R/R_S = 2.2$).

The cap or column opening angle is determined by the model of the magnetic field geometry near the surface, and the magnetosphere and distant accretion flow interaction (cf. Ghosh and Lamb 1979; Arons and Lea 1980). For a centered, nonrelativistic magnetic dipole configuration at the stellar surface, interacting with an accretion disk at the Alfvén surface, the marginally closed last field line gives a polar cap or column opening half-angle $\Theta_0$ given by a variant of the general criterion $\rho v_r v_\phi \sim B^2/4\pi$ (Ghosh and Lamb 1979), specialized to an $\alpha$-disk in regime (*b*) of Shakura and Sunyaev (1973),

$$\sin\Theta_0 = 0.189\alpha^{1/61}\dot{m}^{8/61}m^{-9/61}(R/R_S)^{-59/61}B_{12}^{-20/61}\,, \quad (1)$$

where $\dot{m}$ is the accretion rate in critical (Eddington) units, $m$ is the mass in solar units, and $\alpha$ is the disk viscosity parameter. This expression, for typical XRP fields of $B_{12} \approx 1$ and other parameters of order unity, gives opening half-angles of order 5°–10°. General relativistic corrections to the dipole geometry (Wasserman and Shapiro 1983) would modify this angle estimate, but the other assumptions, such as thin disk geometry, thin transition zone, centered field, and so on, are likely to be equally important, and we shall neglect any such corrections here. The largest uncertainty by far, of course, is the assumption of a dipole geometry, and in fact we shall below find reason to suggest that the field geometry is likely to be more complicated. For this reason, we shall use equation (1) as a rough estimator of the dipole component only.

## III. RESULTS

### *a) Cap Models*

In this type of model, the emission region lies flush on the surface of the neutron star, and consists of a spherical section (cap) symmetrical about the magnetic axis. We usually assume two symmetrically opposite caps. We have made calculations for stellar radii of 4, 3, 2, and 1.6 $R_S$ and opening half-angles of 5° corresponding to fields of order $B \approx 5 \times 10^{12}$ G, if the size of the emission region is given by the dipole component.

Figure 1 shows the spectrum for a star of $R = 4\ R_S$ for various values of the polar angle $\Theta$ with respect to the magnetic axis at infinity. The curves have been offset from each other in order to accentuate the limb-darkening behavior. For this radius, the flux-angle behavior is qualitatively of the usual form (i.e., flux decreasing as the angle $\Theta$ with respect to the magnetic axis increases), although because of the general relativistic (GR) corrections the behavior is not quite proportional to cos $\Theta$. The top curve (0°) shows the true flux for that angle, and successively lower curves (larger angles) are multiplied by an extra factor of $10^{-1/2}$ with respect to the previous curve. We show 21 angles going from 0° to 180° in steps of 9°. The cyclotron line appears as a negative (absorption-like) feature at an observer energy of about 38 keV, with a slight shifting toward higher energies as one samples angles closer to the magnetic axis. This is because of the Doppler and recoil effects in the resonant denominators of the scattering cross section, which is responsible for the cyclotron feature (i.e., this is not a true absorption, but represents photons being scattered out of the

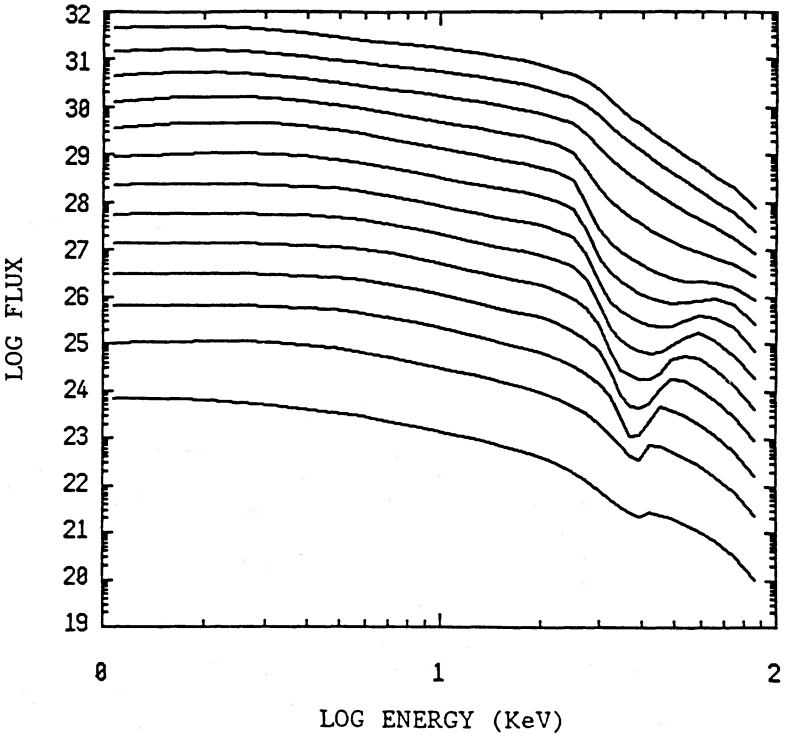


FIG. 1*a*

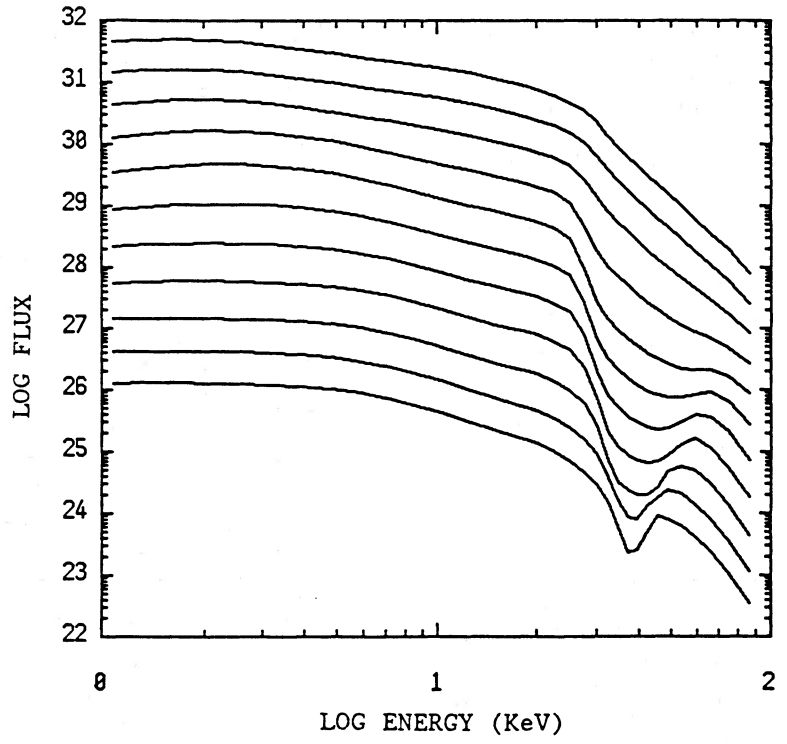


FIG. 1*b*

FIG. 1.—Spectral flux of a cap of $R/R_S = 4$ and opening half-angle $\Theta_0 = 5°$. The ordinate is log (photons $cm^{-2}$ $sr^{-1}$ $keV^{-1}$), and the abscissa is log (photon energy in keV). (*a*) Spectrum for one pole only; (*b*) spectrum for two symmetrically located poles. The various curves give the flux at various angles $\Theta$ between the magnetic axis and the line of sight at infinity. The top curve here is $\Theta = 0°$, showing the real flux value. The next one down is 9°, and the flux has been multiplied by $10^{-1/2}$. This staggering is in the direction of the flux decrease, which it accentuates, and is introduced for easier visualization. The next flux curve down is 18° multiplied by $(10^{-1/2})^2$, and so on, at intervals of 9°. For two poles (*b*) there is a reflection symmetry about $\Theta = 90°$. Note that in (*a*) the curves go down to 108°, i.e., below the flat-space horizon of 90° + 5°. This is because there is some light bending even for $R/R_S = 4$. The cyclotron line is seen as a depression (cf. MN1), and for this radius the cyclotron line blue-wing shoulder (to the right of the depression) for the two-pole configuration (*b*) which is presumably observed increases its energy for an increasing flux, which is the flat-space limb-darkening law expected for caps (or slabs). Physically, the high fluxes are achieved for photons which originate in directions close to along the magnetic axis.

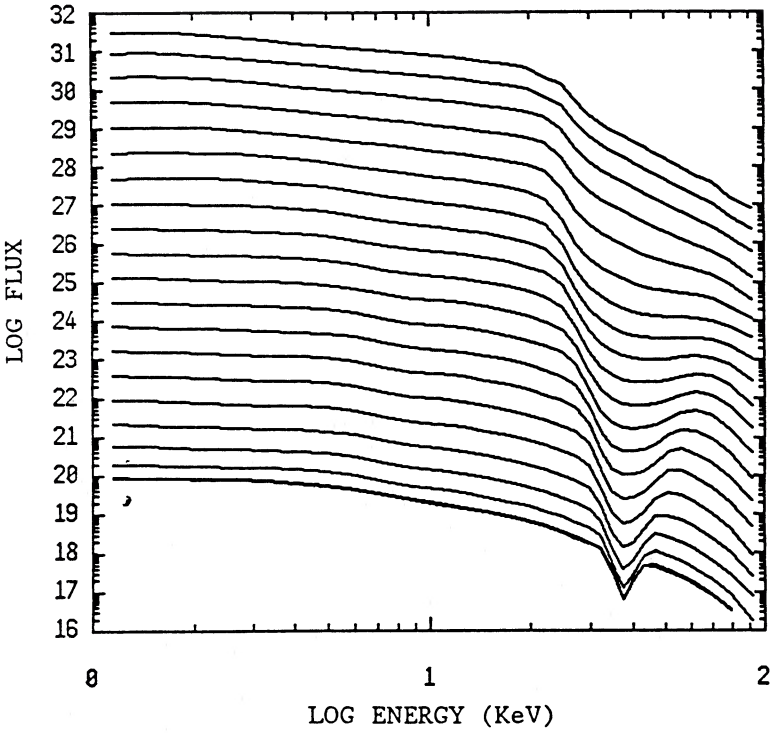


FIG. 2*a*

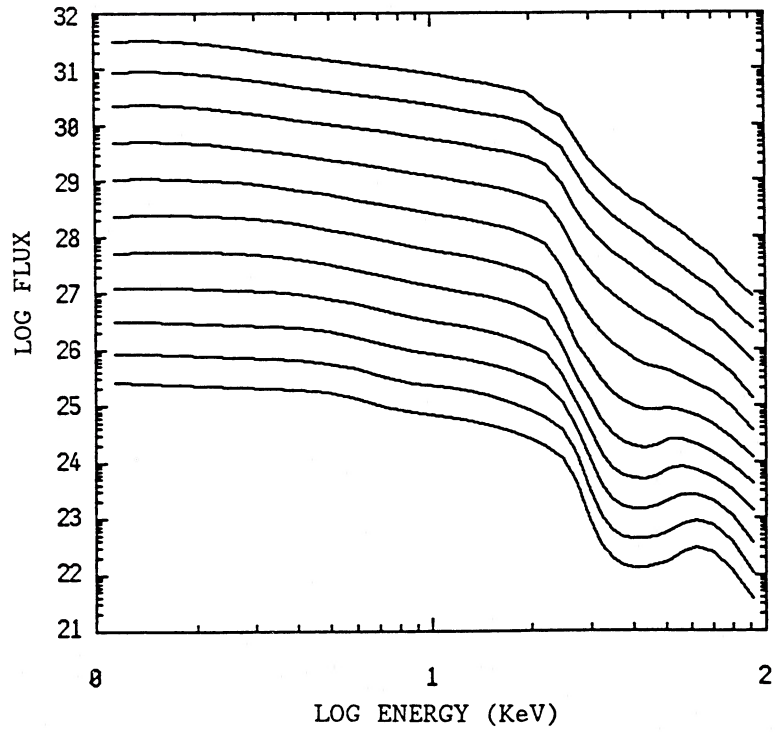


FIG. 2*b*

FIG. 2.—Spectral flux for a cap of $R/R_S = 1.6$ and opening half-angle $\Theta_0 = 5°$. Conventions are as in the previous figure. (*a*) One-pole spectrum; (*b*) two-pole spectrum. For this small radius the light bending is extreme, as seen from the number of curves in (*a*) going beyond 90°, in fact all the way down to 180°. The other remarkable effect of the light bending is that now the limb-darkening behavior of the two-pole configuration (*b*) is the opposite of that for the larger radius caps: the cyclotron line blue-wing energy decreases, instead of increasing, with increasing flux. This inversion occurs because the high fluxes arise from photons which originate in directions closer to perpendicular to the magnetic axis, and are bent into the line of sight. In effect, one is mainly seeing the hidden pole.

resonance core; cf. MN1). Also, one sees that the blue wing, or shoulder, of the line becomes broader and more shifted toward higher energies as the angle approaches 0°, i.e., as one views the radiation along the field. This is again caused by the normal Doppler effect. Qualitatively, these effects appear also in the flat-space calculations of MN1, the GR effects introducing only modest quantitative changes. This is not surprising, since at $R/R_S = 4$ one would expect a behavior close to the usual one. Our light-bending code was of course tested by, among other things, verifying that for very large radii, such as $R/R_S = 100$, the flat-space behavior was accurately reproduced. In particular, we find that, as in the flat-space caps of Paper I, the line blue shoulder energy increases with increasing observed flux, as one samples different angles.

As one decreases the radius, the photon orbits emergent from the caps become more and more bent before reaching the observer, so that for observer angles at infinity close to 90° one receives an increasing proportion of photons that originally were emitted at small angles, while near the observer angle 180° (which because of the two-cap symmetry is the same as observer angles close to 0°), one observes an increasing proportion of photons that originally were emitted at angles nearer to 90° with respect to the magnetic axis. The result of this is that the previously discussed near–flat-space limb-darkening behavior changes, and for the smaller radii $R/R_S \lesssim 2$ it becomes inverted. That is, for the cap models at smaller stellar radii, the line blue-wing energy decreases with increasing observed flux. Note that, both here and above, we understand by line blue-wing energy either a blue-wing energy centroid or, alternatively, the peak or maximum of the blue wing. This inverted limb-darkening behavior is seen in Figure 2, which is similar to Figure 1 but for a radius $R/R_S = 1.6$. For an intermediate radius like $R/R_S = 3$, not shown here, the behavior is still essentially that of Figure 1, although showing a tendency toward the behavior seen in Figure 2. The transition radius between the behavior of the type of Figure 1 (quasi–flat space) and that of Figure 2 (extreme relativistic) occurs at about 2.2 $R_S$.

The pulse shapes seen by a distant observer depend on the inclination angles $i_1$ and $i_2$ between the rotation axis and the observer and between the rotation axis and the magnetic axis. In order to see the effects of a varying stellar radius on the pulse shapes, we have plotted in Figure 3 the pulses that would be seen for an arbitrary set of inclination angles $i_1$, $i_2 = 60°$, 45°. The radius $R/R_S$ is 1.6, 2, 3, and 4 from left to right, while the different curves are the observed flux at different photon energies, increasing from bottom to top. The observed cyclotron energy is the third curve from the top. The most striking trend in Figure 3 is the decreasing degree of pulse modulation as the stellar radius decreases from right to left down to about $r \sim 2\ R_S$. These pulse shapes were all computed for a constant opening half-angle of 5° for the polar cap. This occurs for all energies, although it is less pronounced at the cyclotron energy, where the beaming is always stronger than in the continuum (see MN2). This confirms the similar demodulation for decreasing radius found for the bolometric or monochromatic radiation from caps, when the intensity at the source is angle-independent (see Paper I). In the present case, the intensity at

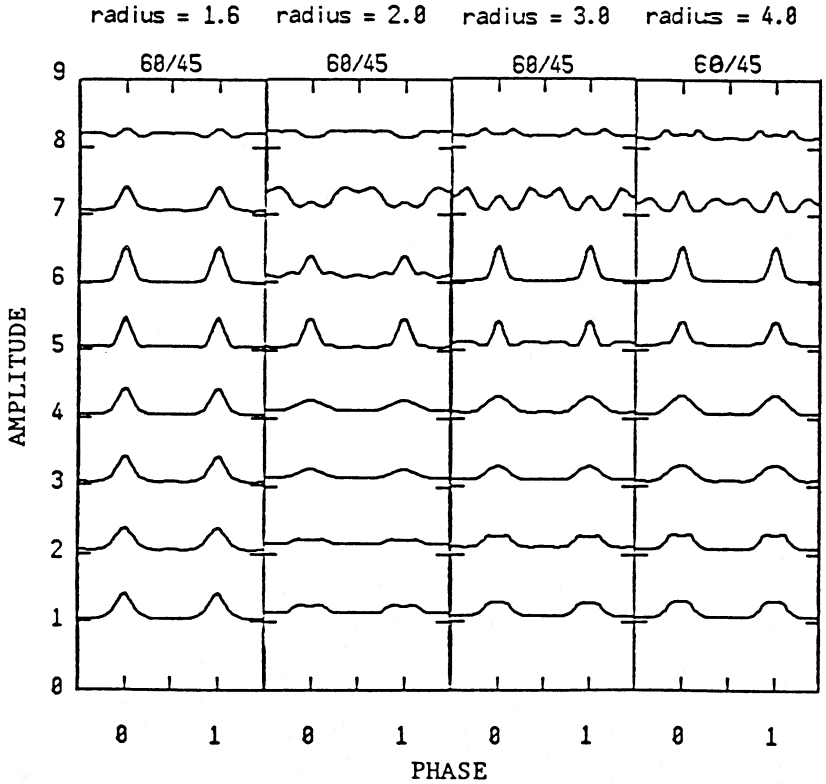


FIG. 3.—Observed pulse shapes for cap models of varying radii, $R/R_S = 1.6$, 2, 3, and 4, from left to right. The opening half-angle is $\Theta_0 = 5°$. The abscissa is the pulse phase. The ordinate is the flux amplitude seen for a particular observer, which in this example is characterized by inclination angles $i_1$, $i_2$ between the line of sight and the rotation axis and between the rotation axis and the magnetic axis taken to be 60°, 45°. The flux amplitude is normalized to the total-angle integrated flux emitted at the star. Eight photon energies are shown in increasing order from the bottom: 1.6, 3.8, 9, 18, 29, 38, 52, and 85 keV, the (observed) cyclotron energy being the third from top.

the source is no longer isotropic but is already beamed at the surface, owing to the anisotropic magnetic opacities (see MN1), but the GR demodulation effect is quite able to flatten out significantly the cap model frequency-dependent pulse profiles for radii less than about 3 $R_S$.

However, for $R \lesssim 1.8\ R_S$ the 180° backward beaming is sufficiently strong to remodulate the pulse shapes (see panel 1 of Fig. 3). This effect is also seen in the calculations of Pechenick, Ftaclas, and Cohen (1983) and Paper I, but notice that in these references the remodulation starts to occur at smaller radii than here ($R \approx 1.6\ R_S$). The difference is that in the present paper the input function is already anisotropic (beamed) owing to magnetic effects in the transfer, whereas in the previous references an isotropic input function was assumed. Because of the initial anisotropy, the demodulation we see here is quantitatively less, and the remodulation also starts to show up at somewhat larger radii than there.

### *b) Column Models*

In this type of model, the emission region protrudes above the stellar surface, having the shape of a section of a conical surface extending between the stellar radius $R$ and an upper radius $R_c > R$. The cone axis is the magnetic axis, and we assume two such oppositely located columns. For columns satisfying $\Delta R/R \ll 1$, as assumed here, the radial direction of the lateral emitting surface approximates quite well the shape expected for a dipole field. We assume that the top surface does not emit significantly, an assumption which simplifies the radiative transfer considerably, and which can be justified partially by the results of approximate radiation hydrodynamic calculations involving a radiation shock front (e.g., Wang and Frank 1981; Basko and Sunyaev 1976; Kirk 1985). The height of the emission column, $R_c$, is chosen here arbitrarily.

The largest effect of the choice of $R_c$, aside from the normalization factor on the total escaping luminosity, is reflected in the visibility of the opposite (hidden) column. For upper column radii $R_c$ larger than the generalized focusing radius $R_\pi$ (Paper I), which is a function of the stellar radius $R$ and the opening half-angle $\Theta_0$, the opposite column can be seen, i.e., there is deflection through $180° - \Theta_0$. For $R_c$ less than $R_\pi$, the opposite column is not seen, which leads to a pulse minimum (since the front column cannot be seen either, because of our assumption of no emission upward, only sideways).

In Figure 4 we show the column spectra for the various polar angles, calculated for a star of $R = 4\ R_S$, and an opening half-angle of 5°. The height $R_c$ is 4.4 $R_S$, which is below the focusing radius $R_\pi$. The "usual" flat-space limb-darkening behavior for columns is seen, which is something roughly like flux proportional to $I(\Theta) \sin \Theta$ (see MN1), modified somewhat by GR effects. That is, since the flat-space flux is maximum perpendicular to the column axis, and the line blue-wing energy is smallest and narrowest in those same directions, we have a decreasing line blue-wing energy with increasing flux. Again, we have highlighted this effect by offsetting the curves by decreasing powers of $10^{-1/2}$, the top curve (90°) giving the actual value.

For decreasing radii there is an increasing amount of light bending, until the radiation of one column is deflected over angles larger than $180° - \Theta_0$, when the hidden column becomes visible, provided that its upper radius $R_c$ is above the focusing radius $R_\pi$. In Figure 5 we show what happens for a

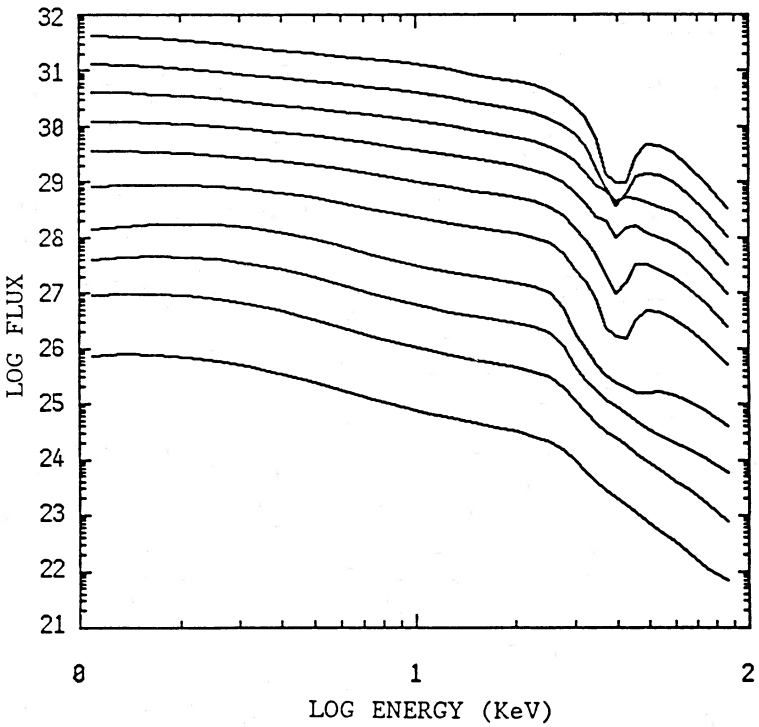


FIG. 4.—Spectral flux for a column model of $R/R_S = 4$, column upper radius $R_c/R_S = 4.4$, and opening half-angle $\Theta_0 = 5°$. Conventions are as in Fig. 1, except for the fact that for this fairly nonrelativistic column, the small angles with respect to the rotation axis correspond to small fluxes, and the maximum flux is around 90°. At angles less than 5°, which is the opening half-angle, there is no emission. The two-pole configuration only is shown here. Note the flat-space limb-darkening behavior of a column; that is, the general trend is that here the cyclotron line blue-wing energy decreases with increasing flux. This is valid for all curves except the two top ones, where because of a combination of partial light bending and the fact that the column walls are conical the behavior begins to reverse.

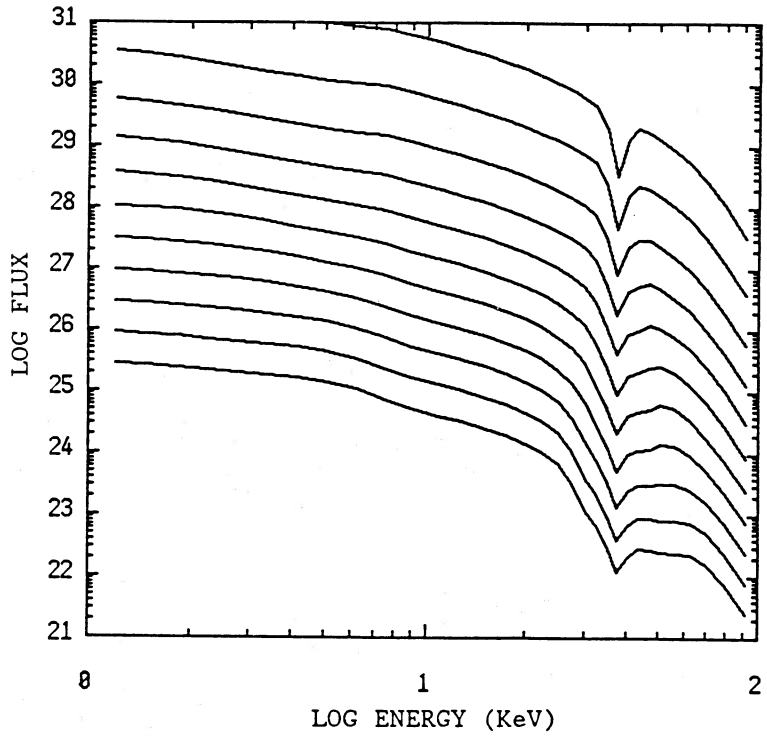


FIG. 5.—Spectral flux for a column of $R/R_S = 1.6$, upper column radius $R_c/R_S = 1.7$, and opening half-angle $\Theta_0 = 5°$, two-pole configuration. Conventions are as in Fig. 1. In this small-radius case, the high fluxes again are in the directions close to the rotation axis, so that the top curve of highest flux is at 0°. While this high flux is given by photons which originally were emitted closer to perpendicular to the magnetic axis, they have been strongly bent around, so that at infinity they are traveling close to parallel to the magnetic axis. This also leads to an inversion of the column limb-darkening law, in the four or five highest fluxes, where the centroid of cyclotron line blue-wing energy shows a trend of increasing with increasing flux.

column case of stellar radius $R = 1.6\ R_S$ and column upper radius $R_c = 1.7\ R_S$ if the opening half-angle $\Theta_0$ is equal to 5°. For these values, the focusing radius $R_\pi$ coincides with the stellar surface. As occurred with the caps, for the very small radii one observes an inversion of the limb-darkening behavior with respect to what it does in flat space. One sees that for an observer at infinity, such a small-radius column would show an increasing line blue-wing energy for an increasing flux, as a function of angle, with a pulse or flux maximum at directions along (not perpendicular to!) the magnetic axis. This extreme relativistic column behavior is the opposite of the flat-space column behavior, but it is qualitatively the same as the flat-space cap behavior. Similarly, an extreme relativistic cap behaves qualitatively similarly to a flat-space column. This qualitative similarity refers to the limb-darkening law in the continuum, and to the line energy shift with flux variation. There is another aspect, however, in which a nonrelativistic cap is unlike a relativistic column, and that is discussed next.

The column pulse-shape behavior with decreasing stellar radius is only partially similar to that of the caps. Starting from the large radii, the pulse modulation initially decreases with decreasing stellar radius, as it does in the caps. However, the effect of the focusing radius introduces a new effect, which is that whenever the column upper radius is above the focusing radius (which can happen for the small stellar radii, since the focusing radius diminishes with diminishing stellar radius), a spike appears at the phase angle corresponding to the line of sight close to the magnetic axis. This phase angle is that of the pulse minimum at large radii (the maximum occurring when one looks at right angles to the axis), but at the lower radii one sees at this phase angle this spike, which is now a pulse maximum, instead of a pulse minimum. The pulse maximum appears as a spike of width approximately given by the projected column opening half-angle. This spike does not appear at all inclination angles $i_1$, $i_2$, but only at those for which the line of sight comes within an angular distance of the magnetic axis which is less than about the column opening half-angle. It is most prominent when $i_1 + i_2 = 90°$. In Figure 6 we show the pulse shapes for various stellar radii, $R/R_S$ going from 1.6, 2, 3, to 4 from left to right. The pulse shapes are given from low frequencies (*bottom*) to high frequencies (*top*), where the cyclotron energy is the third curve from the top. Again we have used for illustration purposes a particular representative set of inclination aangles $i_1$, $i_2$, and an opening half-angle of 5°. The column height is here $\Delta R/R = 0.1$. For the two largest stellar radii, the column upper radius is smaller than the gravitational focusing radius, and therefore at phases where one looks close to the magnetic axis one sees a minimum: the near column shows its nonemitting top, and the hidden column is not focused into our line of sight. For the two smallest radii, the column height is larger than the gravitational focusing radius, and the opposite (hidden) column is beamed into our line of sight, leading to a pulse maximum at phases close to the magnetic axis. The exact value of $R_c$ does not influence the pulse shape strongly; what does is whether it is above or below $R_\pi$, the gravitational focusing radius. Since the opening half-angle is small, the 180° maximum found at small radii is similarly narrow or spikelike. At large radii, however, the pulse maxima are rather broad, as is typically the flat-space behavior of magnetized columns (cf. MN2). This is a combination of the smoother angular dependence of the opacitiy perpendicular to the field, combined to the sin $\Theta$ effective surface area factor.

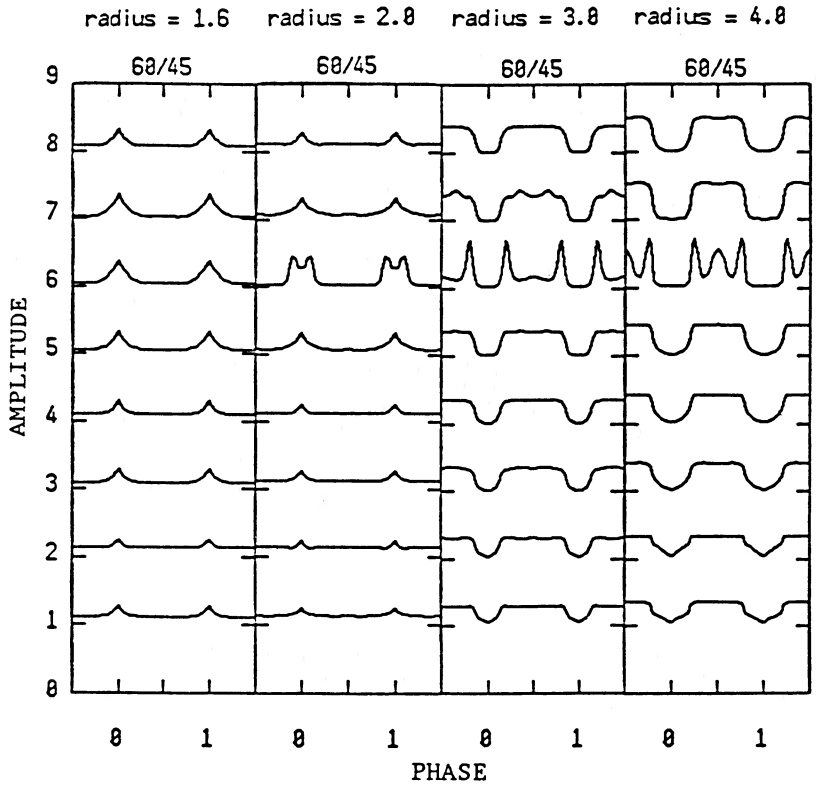


FIG. 6.—Column pulse shapes for an opening half-angle $\Theta_0 = 5°$ for radii $R/R_S = 1.6$, 2, 3, and 4, from left to right. Conventions are as for Fig. 3, and the inclination angles are $i_1, i_2 = 60°, 45°$. The eight curves give increasing photon energies from bottom to top, the cyclotron line being the third from the top. Notice that the pulse minimum, which appears at phase zero for the less relativistic configurations (angles close to the magnetic axis), becomes a pulse maximum in the more relativistic configurations, owing to the relativistic light bending which deflects the photons. Note also the narrowness of this relativistic pulse maximum in this case, which is of the order of the opening angle.

### c) *Effect of Larger Opening Half-Angles*

A larger opening angle leads to an earlier inversion of the limb-darkening behavior, that is, it starts to occur at larger radii the larger the opening angle is, since the photons need to be bent through a smaller angle. For the same radius, the inverted limb-darkening behavior becomes more pronounced the larger the value of the opening half-angle. This is illustrated in Figure 7 for a column model of radius $R = 1.6\ R_S$, $R_c = 1.7\ R_S$ and opening half-angle $\Theta_0 = 40°$, which gives the spectrum for different observer angles. One sees that the inverted limb-darkening behavior of Figure 6 is now extended to a larger number of angles. A similar effect occurs for the cap models, where, however, the inversion is of the opposite sign.

The effect of increasing the opening half-angle on the cap pulse shapes is simply to broaden the maxima and sharpen the minima. On the other hand, the effect of changing the opening half-angle on the column pulse shapes is to increase the width of the pulse troughs (minima) at large stellar radii, and to increase the width of the pulse maxima at small stellar radii (i.e., where at 180° the spike becomes a broader pulse maximum, of width given by the opening half-angle). The broader this is, the larger is the chance that the line of sight samples this maximum, so that it becomes more probable for a randomly oriented observer of given $i_1, i_2$ to see this phenomenon as a pulse maximum. In Figure 8 we show for the single radius of $R = 1.6\ R_S$ the column pulse shapes seen by five different random observers, given by the five different sets of curves from left to right, identified by the values of $i_1, i_2$ shown at the top. The opening half-angle is here 40°, which gives a significant pulsed fraction and degree of modulation, despite or rather thanks to the very strong gravitational light bending. The cyclotron line blue-wing (high-energy shoulder) centroid as a function of phase is shown in Figure 9, for the $R/R_S = 1.6$ and $\Theta_0 = 40°$ column model, showing the limb-darkening behavior discussed above, namely, an increasing line energy for increasing flux. The flux maximum is at $\phi = 0$, the minimum at $\phi = 0.5$. This behavior is qualitatively the same as observed in Her X-1 (Voges *et al.* 1982).

## IV. DISCUSSION

The observational evidence in Her X-1 indicates that the cyclotron line blue-wing energy increases with increasing flux (see Voges *et al.* 1982). Also, the pulse shape is significantly modulated and moderately broad at all photon energies for which the object is detected in X-rays (see Pravdo *et al.* 1978; Trümper *et al.* 1978). In order to satisfy the Her X-1 observations, we need therefore to invoke one of two types of models discussed here. We must have either (1) a large-radius neutron star emitting via a polar cap geometry with a "standard" small opening angle (see Fig. 1 and the right-hand panel of Fig. 3), since these will give the right limb-darkening law and an adequate amount of pulse modulation and width (this was in fact the model suggested in MN1 and MN2 on the basis of our previous flat-space calculations), or (2) a small-radius neutron

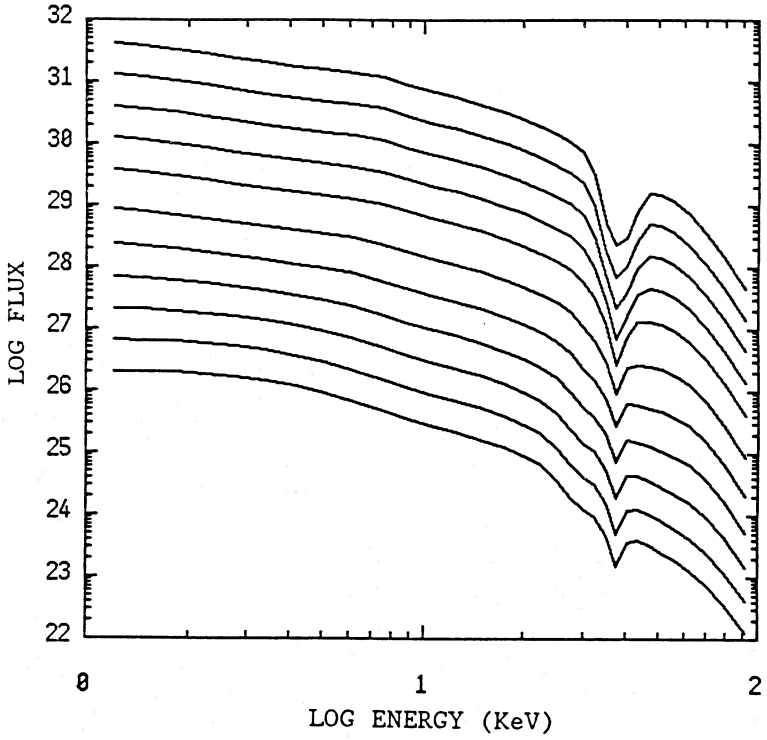


FIG. 7.—Spectral flux for a column model of larger opening half-angle $\Theta_0 = 40°$ and small radius $R/R_S = 1.6$, upper column radius $R_c/R_S = 1.7$, and other conventions as in Fig. 1. Here again, because of light bending, the high fluxes correspond to angles closer to the magnetic axis, starting with 0° for the top. The two-pole configuration is shown. The inverted column limb-darkening behavior is here much more obvious, the cyclotron line blue-wing energy increasing with increasing flux.

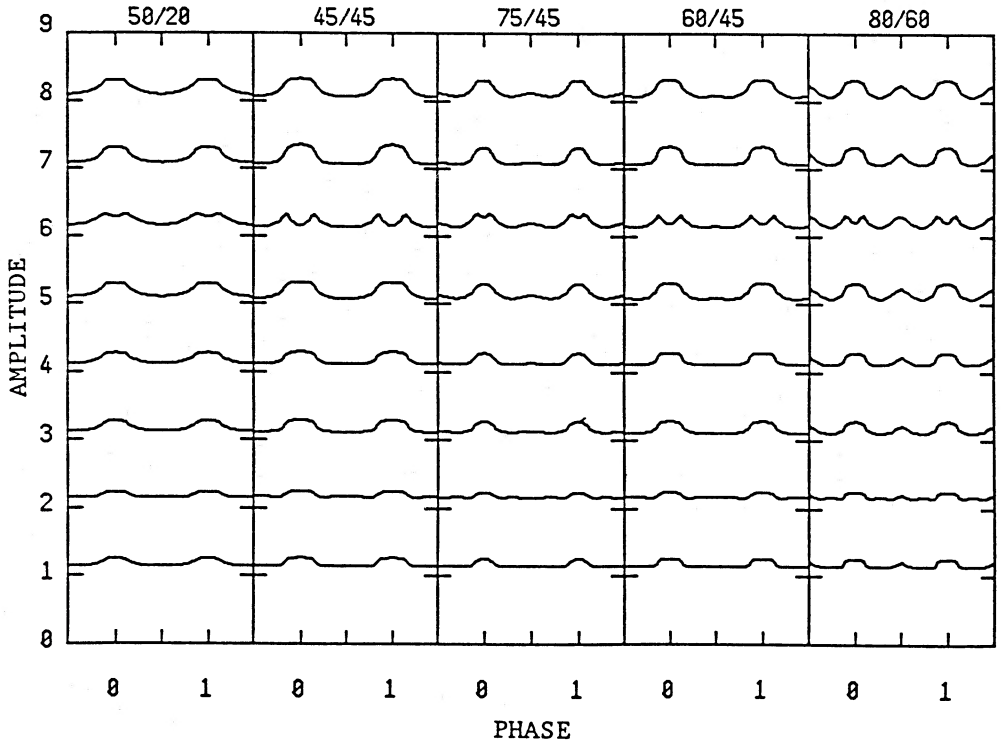


FIG. 8.—Column pulse shapes for an opening half-angle $\Theta_0 = 40°$ and the single radius $R/R_S = 1.6$. The five panels (*left to right*) are for various inclination angles $i_1$, $i_2$, indicated along the top. The photon energy corresponding to the cyclotron line is the third curve from the top. Note that, since the configuration is very relativistic, the pulse maximum comes at phases corresponding to angles close to the magnetic axis. Note also the broader peak structure here than in the left panel of Fig. 6, because of the larger opening half-angle of 40° taken here.

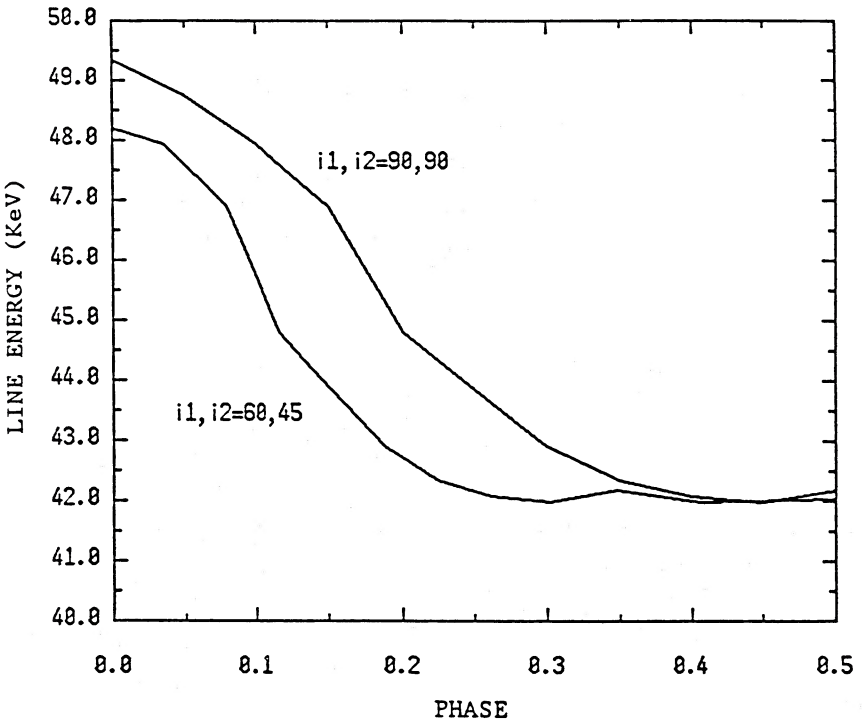


FIG. 9.—Cyclotron line blue-wing shoulder energy $E_s$ as a function of phase, for the small-radius, large opening angle column model of Figs 7 and 8, when the inclination angles $i_1$, $i_2$ are taken to be 90°, 90° and 60°, 45° as examples. Phase zero is high flux, phase 0.5 is low flux, and the limb-darkening law of increasing line energy with increasing flux is present. This agrees qualitatively with the observed behavior in Her X-1.

star emitting via a column geometry with a large, nonstandard opening angle, which can also give the right limb darkening and adequate pulse widths and modulation (see Figs. 7 and 8).

The choice between these two simplified X-ray pulsar models cannot be made observationally or by adding more realistic details to our atmosphere models, unless one performs a fully fledged two- or three-dimensional magnetized radiation hydrodynamic calculation. Such calculations are extremely difficult to perform and to interpret. The current evidence, supported by previous very idealized numerical calculations (Basko and Sunyaev 1976; Wang and Frank 1981) as well as simple analytic solutions (Kirk 1985), suggests that for luminous X-ray pulsars such as Her X-1 one can possibly expect a radiation mediated standoff shock to protrude above the stellar surface. This would suggest that a column geometry, radiating principally sideways (perpendicular to the field), may be more realistic. Such configuration in flat space, or for large radii, would radiate like a fan beam and give the wrong limb darkening (see MN1). In addition, there is indirect evidence related to the 35 day period in Her X-1 indicating that the beaming geometry may be of the pencil type (see Trümper 1986). This would be compatible with our large radius, small opening angle cap models, as concluded in MN1 and MN2. On the other hand, it would also be compatible with our low-radius, large opening angle column model presented here, which because of the large light bending ends up radiating at infinity as a pencil beam, although at the emission surface it starts out as a fan beam. This latter option would be more satisfying from the point of view of the present tentative dynamic calculations.

For low-luminosity accreting pulsars (less than $10^{35}$ ergs $s^{-1}$, say) the radiation pressure is unimportant, so that a radiation shock is not present, although collisionless processes could still induce a shock leading to a column geometry. Alternatively, if these processes are insufficient, Coulomb or nuclear collisions would decelerate the matter in the dense lower atmosphere, leading to a cap (or slab) model (Harding *et al.* 1984). Unfortunately, no cyclotron line data are available so far for this class of objects. A cap model would give the right pulse modulation, but if the neutron star radius is small, as argued above, it would give an inverted limb-darkening law. This would in fact be a prediction for the Coulomb decelerated, low-luminosity accreting pulsars, which future pulse-phase cyclotron data may be able to test.

Of course, a detailed fit to the observed pulse profiles would require a more detailed model than our simple columns represented as homogeneous, symmetric sections of cones. From the dynamic calculations one may infer an emission mound, rather than a simple cylinder or a cone. While the dominant component of the radiation would be emitted sideways, this would still give some emission upward. If we added on top of our present column further, narrowing column components, or allowed some upward emission in an ad hoc manner, one would add a narrower pulse component on top of the somewhat square pulses seen in Figure 8, which would further improve the resemblance to observed pulse profiles. Thus, while the pulse widths of Figure 8 are reasonable for Her X-1, the degree of modulation could be improved from 20% to 30% as seen in that figure to a value closer to $\lesssim 50\%$ in the band 16–33 keV, as observed (Maurer *et al.* 1979), with the addition of such additional components. Also, plasma instabilities may render the emission region inhomogeneous, introducing a random component into the pulse shapes. Furthermore, the field lines may be unequally loaded in the azimuthal direction, or else the magnetic dipole component may not be star-centered or symmetrical, all of which could lead to asymmetric

pulse profiles. All of these improvements would require extensive further work. However, it is apparent from the present calculations that the gross features of observed pulse shapes can be reasonably reproduced with the general class of large opening half-angle, small-radius column models.

The current status of neutron star equation-of-state calculations (see Baym and Pethick 1979) indicates that the stiffer equations of state could lead to a neutron star radius corresponding to about 4 $R_S$. On the other hand, one requires a very soft equation of state (e.g., including the effect of pionization) to give radii as small as 1.5–1.6 $R_S$. These are within the realm of what might be called the less speculative equation-of-state calculations; a number of calculations have also explored beyond this range, but need not be considered here. There is, in addition, observational evidence (mediated by model calculations) about the radius of other types of neutron star sources, in particular X-ray bursters. These are believed to be low magnetic field neutron stars. Extensive investigations have led to estimates of the effective emitting area, which, when coupled to the current mass estimate of about 1.4 $M_\odot$ derived for XRPs, would be compatible with a radius less than 2 $R_S$ Schwarzschild radii, while the value of 1.5 or 1.6 has been invoked fairly often (see Joss and Rappaport 1984; Fujimoto and Taam 1986; Fujimoto 1987; Sztajno *et al.* 1987). There is no reason to expect that the presence or absence of a strong field would physically affect the radius, if the mass is the same (the mass equivalent of the field energy is negligible compared with the total mass, and in any case, the field may not penetrate below the crust). There have been other investigations, concerning the accretion torque estimates derivable from the period derivatives of XRPs (Wasserman and Shapiro 1983), which indicate that under the dipole assumption a lower radius (6–8 km) produces a better fit. There are thus at least two other independent (albeit still inconclusive) lines of investigation which suggest that neutron star radii may be on the low side (see Mészáros and Riffert 1987). The value of our relativistic best-fit model, $R/R_S = 1.6$, is in very good agreement with these other estimates.

We seem therefore to be led toward a preference for the low-radius model, which in order to fit the cyclotron line shifts of high-luminosity objects must be of the column accretion type, and in order to fit the pulse widths and modulation degree must have a somewhat larger than usual opening angle (the latter also improves the line-shift fit, but is not as crucial as the first one). A larger opening angle would suggest, if equation (1) is applicable, a lower dipole component of the magnetic field. Since direct observations already give us a large ($>4 \times 10^{12}$ G) value for the surface field, this would indicate either (1) that some of the assumptions on which equation (1) is based do not apply here or (2) that there is a nondipole component to the surface field. There have in fact been suggestions (Lamb 1978) that besides a dipole component Her X-1 may require a non-dipole contribution. In this case, the dipole would be somewhat lower, and the surface field strength observed would include a sizable higher multipole contribution. The higher multipole field lines would have a larger opening angle, and would be plasma-loaded if plasma or hydromagnetic instabilities transferred material onto them.

On the basis of the theoretical arguments and observational evidence discussed in this section, and the theoretical cyclotron line phase-shift and light-curve calculations presented in § III, we conclude that the best-fit model for high-luminosity accreting pulsars such as Her X-1 is obtained for a small-radius star ($R/R_S < 2$) with a moderately large opening half-angle ($\Theta_0 \lesssim 40°$), emitting in a column-type geometry.

This research was partially supported through National Science Foundation grant AST 8514735 and the Deutsche Forschungsgemeinschaft. We are grateful to O. Furmanski for computational assistance.

## REFERENCES

Arons, J., and Lea, S. 1980, *Ap. J.*, **235**, 1016.
Basko, M. M., and Sunyaev, R. A. 1976, *M.N.R.A.S.*, **175**, 395.
Baym, G., and Pethick, C. 1979, *Ann. Rev. Astr. Ap.*, **17**, 415.
Fujimoto, M. Y. 1987, *Ap. J.*, **324**, 995.
Fujimoto, M. Y., and Taam, R. E. 1986, *Ap. J.*, **305**, 246.
Ghosh, P., and Lamb, F. K. 1979, *Ap. J.*, **234**, 296.
Harding, A. K., Mészáros, P., Kirk, J. G., and Galloway, D. J. 1984, *Ap. J.*, **278**, 369.
Joss, P. C., and Rappaport, S. A. 1984, *Ann. Rev. Astr. Ap.*, **22**, 537.
Kirk, J. G. 1985, *Astr. Ap.*, **142**, 430.
Lamb, F. K. 1978, review presented at the International Conference on Cyclotron Lines in Accreting Neutron Stars, MPE, Garching.
Maurer, G. S., Dennis, B. R., Coe, M. J., Crannell, C. J., Cutler, E. P., Dolan, J. F., Frost, K. J., and Orwig, L. E. 1979, *Ap. J.*, **231**, 906.
Mészáros, P., and Nagel, W. 1985*a*, *Ap. J.*, **298**, 147 (MN1).
———. 1985*b*, *Ap. J.*, **299**, (MN2).
Mészáros, P., and Riffert, H. 1987, *Ap. J.* (*Letters*), **323**, L127.
Misner, C. W., Thorne, K., and Wheeler, J. 1973, *Gravitation* (San Francisco: Freeman).
Pechenick, K. R., Ftaclas, C., and Cohen, J. M. 1983, *Ap. J.*, **274**, 846.
Pravdo, S. H., Bussard, R. W., Becker, R. H., Boldt, E. A., Holt, S. S., and Serlemitsos, P. J. 1978, *Ap. J.*, **225**, 988.
Riffert, H., and Mészáros, P. 1988, *Ap. J.*, **325**, 207. (Paper I).
Shakura, N. I., and Sunyaev, R. A. 1973, *Astr. Ap.*, **27**, 337.
Sztajno, M. *et al.* 1987, *M.N.R.A.S.*, in press.
Trümper, J. 1986, paper presented at the Workshop on Astrophysics of Time Variability in X-Ray and Gamma Ray Sources, Taos, NM.
Trümper, J., Pietsch, W., Reppin, C., Voges, W., Staubert, R., and Kendziorra, E. 1978, *Ap. J.* (*Letters*), **219**, L105.
Voges, W., Pietsch, W., Reppin, C., Trümper, J., Kendziorra, E., and Staubert, R. 1982, *Ap. J.*, **263**, 803.
Wang, Y-M., and Frank, J. 1981, *Astr. Ap.*, **93**, 255.
Wasserman, I., and Shapiro, S. L. 1983, *Ap. J.*, **265**, 1036.
White, N. E., Swank, J., and Holt, S. 1983, *Ap. J.*, **270**, 711.

P. Mészáros and H. Riffert: 525 Davey Laboratory, Pennsylvania State University, University Park, PA 16802